JOURNAL OF CATALYSIS 135, 518–532 (1992)

Acidity and Catalytic Activity of MeAPSO-34 (Me = Co, Mn, Cr), SAPO-34, and H-ZSM-5 Molecular Sieves in Methanol Dehydration

STANKO HOČEVAR* AND JANEZ LEVEC†

*Department of Catalysis and Chemical Reaction Engineering, Boris Kidrič Institute of Chemistry, Hajdrihova 19, P.O. Box 30, 61115 Ljubljana, Slovenia; and †Department of Chemical Engineering, University of Ljubljana, 61000 Ljubljana, Slovenia

Received December 24, 1990; revised October 24, 1991

SAPO-34 and the isomorphously substituted MeAPSO-34 (Me = Co, Mn, Cr) molecular sieves have been synthesized. Temperature-programmed desorption (TPD) profiles and the reaction rates of methanol dehydration have been measured on these samples in comparison with H-ZSM-5. The acidity strength of samples has been determined qualitatively from the temperatures of dimethyl ether desorption peaks, and the following sequence has been obtained: H-ZSM-5 > MnAPSO-34 > CoAPSO-34 > CrAPSO-34 > SAPO-34. The following sequence of catalytic activity has been observed: H-ZSM-5 ⩾ SAPO-34 > CrAPSO-34 > CoAPSO-34 > MnAPSO-34. The selectivities for the formation of low olefines have been observed to decrease rapidly with time on stream for all catalysts in the SAPO-34 and MeAPSO-34 series as a consequence of coking. The highest selectivity to ethene production among these catalysts has been found for MnAPSO-34. © 1992 Academic Press, Inc.

INTRODUCTION

The new petroleum crisis emphasizes again the question of economically feasible routes to production of hydrocarbons from other natural sources. Methanol is one of the largest chemical commodities that can be produced from natural gas, biomass, or from coal via synthesis gas and can be used as a fuel, fuel precursor, and building block for chemicals. The technology of methanol synthesis is mature and there are already some commercial technologies for production of hydrocarbons from methanol (for instance the MTG process of Mobil (*1*)). It is also known that molecular shape-selective acid-catalyzed synthesis of ethene and propene from methanol proceeds over some types of molecular sieves in hydrogen forms, having structures with relatively small pores, like erionite, Zeolite T, chabazite, and ZK-5 (*2*). Unfortunately the coking is rapid on these catalysts. Some modified forms of ZSM-5 with basic additives, such as P (*3*), Mg, Zn, Ca, B (*4*), to reduce the acid strength have been proved to have enhanced selectivity toward lower alkenes and low coking rates, but their activity is greatly reduced.

The coking reactions are a complex function of the distribution of strength and concentration of Brønsted acid centers in a given topology of molecular sieve, as well as of the topology itself, since it determines the possible forms of molecular shape selectivity constraints imposed on the reactants, products, transition states, and molecular traffic. The right combination of all these factors gives the key for the design of active, selective, and stable catalysts for the synthesis of lower olefins from methanol.

Since some topologies of molecular sieves that can give high selectivities for synthesis of lower olefins are already tested (*5*), the task reduces to the design of a proper distribution of acid strength and concentration of Brønsted acid centers in these topologies. The most straightforward way to change the acid strength and concentration of acid

0021-9517/92 $5.00

centers is by isomorphous substitution of elements having different atomic electronegativities, concentration, and distribution in the framework of the molecular sieve.

Recently discovered aluminophosphate molecular sieves (*6*) have opened research in this direction. Aluminophosphates form open crystalline structures having channels and cavities of molecular dimensions. Pure aluminophosphate frameworks are electroneutral, but they can be modified during the synthesis procedure by isomorphously substituting either aluminum or phosphorus, or, in the case of silicon, both of them, thus giving negatively charged frameworks, so called SAPOs, MeAPOs, MeAPSOs, and ElAPOs. These materials have Brønsted acidities in the range between low- and high-silica zeolites (*7*).

The silicoaluminophosphate molecular sieves of the SAPO-34 type (*8, 9*) and with isomorphously substituted nickel, the NiAPSO-34 type (*10*), have been demonstrated to have enhanced selectivity to ethene in the methanol-to-olefins reaction.

The scope of our work was to test the Brønsted acidity and catalytic activity of SAPO-34 molecular sieves containing isomorphously substituted Co, Mn, and Cr (MeAPSO-34). In order to obtain consistent results we have used the same reactant for TPD and catalytic measurements, that is, methanol. We have studied the reaction of methanol dehydration in non-isothermal static conditions (TPD) and in isothermal flow conditions, by measuring catalytic activity in a gradientless catalytic reactor.

EXPERIMENTAL

Samples of MeAPSO-34 (Me = Co, Mn, Cr), SAPO-34, and ZSM-5 were synthesized and transformed into catalytically active forms by standard procedures. The synthesis and preparation of the H-ZSM-5 sample is described elsewhere (*11*). The synthesis and structural characterization of CoAPSO-34 is described in a paper recently published by our group (*12*). Procedures for the synthesis of MnAPSO-34 and CrAPSO-34 were the same as that for the synthesis of CoAPSO-34, except that the chromium was introduced in the reaction system as Cr(VI) oxide (*13*). SAPO-34 was synthesized according to Ref. (*14*). After the synthesis, all samples were characterized by means of X-ray powder diffraction, electron scanning microscopy, thermogravimetry, and quantitative chemical analysis. The template in MeAPSO-34 and SAPO-34 samples was removed by calcination at 823 K for 4 h in a flow of air. Disks with a diameter of 30 mm and thickness of 1.5 mm were pressed from the samples at pressure of 20.3 bar.

A weighed quantity of disks made of each sample (about 0.89 g on average) was used for the catalytic activity test in a Caldwell type continuous stirred tank (CST) reactor (Autoclave Engineers 8-in. catalytic reactor bolted closure with .75-2 MagneDrive II Assembly). The reactant and products were analyzed with a HP 5890 gas chromatograph equipped with a $\frac{1}{8}$-in. diameter, 240-cm-long SS column filled with Porapak T. The oven temperature was 383 K, the TCD temperature was 493 K, and the helium flow rate was 25 cm^3/min. The duration of an analysis was 60 min. The samples were tested at a reactor temperature of 623 K, pressure 1.8 bar, 0.5 ml/min of liquid methanol flow rate, and a reactor impeller speed of 1500 rpm. At the conditions applied, external and internal resistances were equal for all samples.

The TPD profiles ("spectra") were scanned in TG/DTG mode on a Sartorius 4201 electromagnetic suspension balance coupled with a high-vacuum system and a Leybold MSQ 1002 mobile mass spectrometer system including a high-vacuum system with a turbomolecular pump, a gas inlet system, and a Quadrex 200 residual gas analyzer. The apparatus is schematically presented in Fig. 1. About 0.3 g of each sample (on average) was first degassed *in vacuo* at room temperature (298 K) and the weight of

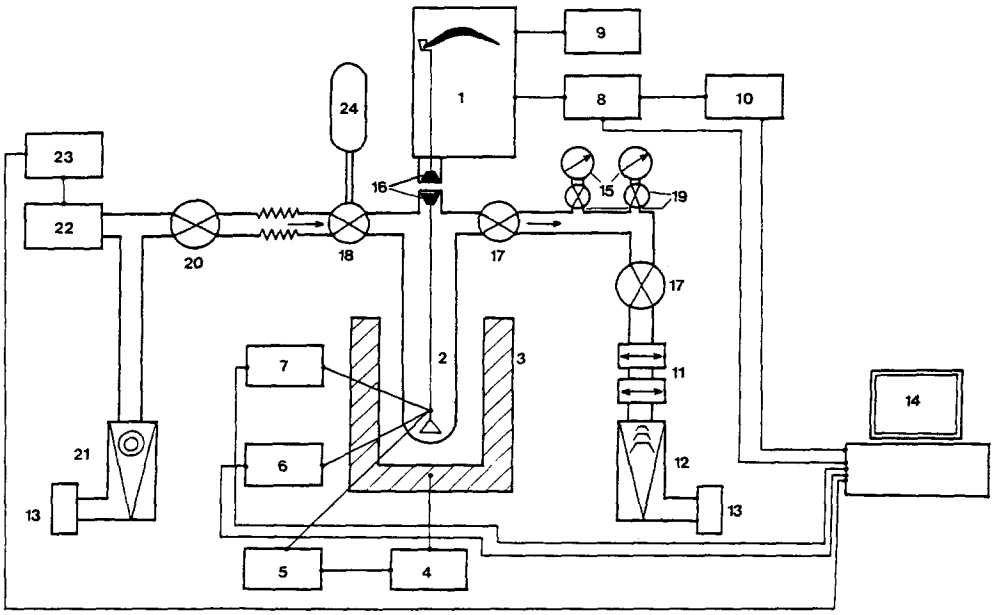

FIG. 1. Block scheme of the apparatus for the TPD measurements. (1) Electromagnetic suspension balance Sartorius 4201; (2) sample housing; (3) Crusilite oven Linseis L82/176; (4) temperature regulator Linseis L70/176; (5) indication thermocouple type S; (6) thermocouple type J; (7) attachment for DTA measurements; (8) weight measuring device (TG); (9) thermostat; (10) DTG device; (11) liquid nitrogen traps; (12) oil diffusion pump; (13) vane rotary vacuum pump; (14) IBM XT, compatible with Burr Brown data acquisition system; (15) vacuum gauge (Pirani, Penning); (16) electromagnet with indicating coil (upper) and static magnet (lower); (17) outlet vacuum vent; (18) inlet microdosing vacuum vent; (19) shutoff vacuum vents; (20) Leybold DW2 pressure reduction system; (21) turbomolecular vacuum pump; (22) Inficon QMS with EM sensor head; (23) Inficon Quadrex 200 control unit; (24) ampule with methanol.

the sample was registered. The temperature was then continuously raised at a rate of 10 K/min until it reached 673 K. At this temperature samples were treated under dynamic vacuum until constant weight was achieved and then cooled to room temperature. The weight of samples was registered again. The vacuum system was then closed and the vapor of dry methanol was introduced into the system at its saturation pressure (about 11.7 kPa). The system was left at this pressure for several hours to attain adsorption equilibrium. The sample weight was registered and the system was then degassed at room temperature for several hours (depending on the sample) until constant weight was achieved. TPD was started with a heating rate of 10 K/min. The sample weight changes were monitored thermogravimetrically in TG/DTG mode and evolved gases were simultaneously analyzed with the mass spectrometer. In the first run for each sample a qualitative analysis of evolved gases was performed. On the basis of this analysis the characteristic lines of parent or fragmentary ions and the scanning parameters were chosen for the second run with a fresh sample in which the composition of evolved gases was determined. The second MS analysis run was performed using an ion chromatographic mode in which 6 characteristic lines of reactant and products were followed simultaneously. The measuring system and the procedure was very similar to that described in Ref. (*15*).

The qualitative MS analysis of evolved gases during the TPD of samples indicated

the presence of methanol, dimethyl ether (DME), water, and hydrocarbons, of which the most interesting are the C_2 hydrocarbons (ethene and ethane). The $m/e = 41$ signal, a typical line for hydrocarbon fragments (*15*), is less informative than the lines characteristic for individual hydrocarbons. A difficulty arises when these lines interfere with lines characteristic for other species. For instance, the line for the parent ion of ethene has $m/e = 28$, which is also present as the line for fragmentary ions of methanol and carbon dioxide as well as the line for the parent ion of nitrogen and carbon monoxide. Fortunately the reaction sequence is such that ethene and ethane desorb at higher temperatures than methanol and the peak belonging to the desorption of the parent ion of ethene with $m/e = 28$ is resolved from the peaks belonging to the fragmentary ions of methanol, having the same m/e value. Moreover, the first run revealed that the peak of the parent ion of ethene ($m/e = 28$) was accompanied by peaks of fragmentary ions of ethene ($m/e = 27$ and $m/e = 26$) not present in the cracking patterns of other gases having the common peak at $m/e = 28$ (*16*).

The cracking pattern and the relative probability of ionization for DME was determined by separate experiments. The relative probability of ionization obtained for DME at a total pressure of 1.3×10^{-4} Pa in the ionization chamber was 2.8.

The quantitative analysis of evolved gases was based on both MS and TG data. The amounts of gaseous species evolved were obtained by integrating the TPD peaks in corresponding temperature intervals using the TGA to calibrate the peak areas (*17*). During TPD the maximum total pressure in the ionization chamber never exceeded 1.3×10^{-3} Pa. In this range of pressure the ion current is linearly dependent on the partial pressure of the gas being analyzed. Since the analyses were performed under identical instrumental operating conditions, the relative peak heights of the mass peaks constituting the cracking patterns of the analyzed gases were reproducible (*18*).

TABLE 1

The SAPO-34 and MeAPSO-34 Chemical Composition Calculated on TO_2 Basis

Sample	Me	Al	Si	P	Si + P	Framework charge
SAPO-34	—	0.49	0.13	0.38	0.51	−0.11
CoAPSO-34	0.08	0.42	0.08	0.42	0.50	−0.16
MnAPSO-34	0.04	0.45	0.11	0.40	0.51	−0.13
CrAPSO-34	0.01	0.48	0.11	0.40	0.51	−0.10
H-ZSM-5		0.05	0.95			−0.05

RESULTS AND DISCUSSION

The chemical composition of samples and the framework charges calculated on the basis of a TO_2 formula (*7*) are given in Table 1.

The TPD spectra of methanol adsorbed on the samples, listed in Table 1, are presented in Figs. 2–6. They differ substantially from one to another, especially in the desorption patterns of dimethyl ether and ethene. The desorption curves of DME are gathered in Fig. 7 (enhanced 10 times for the H-ZSM-5 sample and 100 times for other samples).

The mass balance during TPD experiments is satisfactory, as can be seen from Table 2: within the experimental error, the mass of adsorbed methanol equals the mass of evolved gases during TPD as measured by TG. The composition of evolved gases reveals that about half of the adsorbed methanol desorbs unconverted (the low-temperature peak in TPD spectra). The other half reacts through the formation of DME and, at higher temperatures, through the formation of hydrocarbon. Only traces of DME desorb unconverted (less than 1 mol%) from SAPO-34 and MeAPSO-34 samples. The quantities of desorbed hydrocarbons are small since these molecules are further transformed through hydrocarbon reactions to coke. The evidence for this is the changed color of samples after TPD: the original color of the samples (before TPD) is overlaid

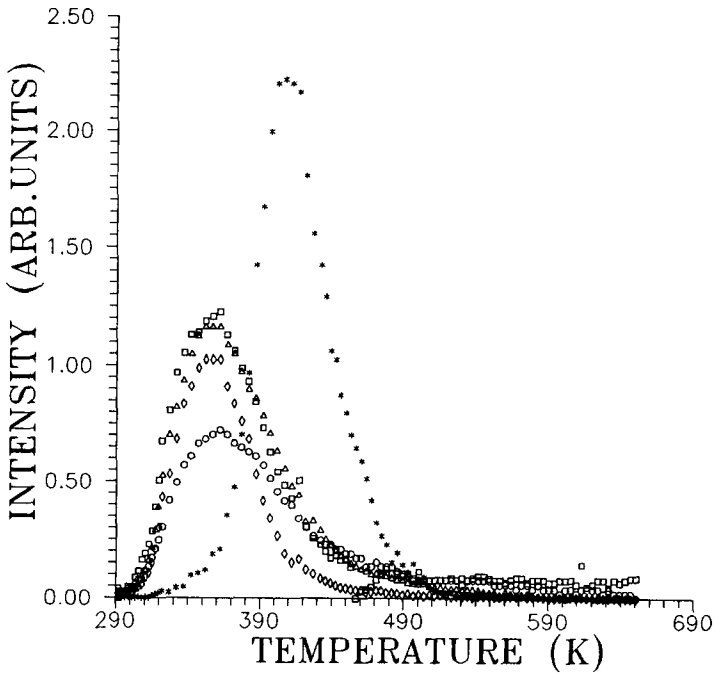

FIG. 2. TPD spectrum of methanol adsorbed on SAPO-34 molecular sieve, obtained by mass spectrometric analysis of evolved gases. (○) m/e = 18 (H_2O^+); (□) m/e = 28 ($C_2H_4^+$) enlarged 5 times; (△) m/e = 29 ($C_2H_5^+$) enlarged 2 times; (◇) m/e = 31 (CH_2OH^+); (∗) m/e = 45 ($C_2H_5O^+$) enlarged 100 times.

by a light to dark gray color. However, the molar fraction of desorbed water is much higher than expected from the stoichiometry of the reaction proceeding during the TPD process:

$$2CH_3OH \rightleftarrows (CH_3)_2O + H_2O \downarrow C_2H_4 + H_2O \downarrow \text{coke} \quad (1)$$

It is interesting to note that during TPD the first quantities of water desorb practically simultaneously with unconverted methanol (see Figs. 2 to 6). The experimental conditions were carefully checked and no readsorption of water was found during the cooling of degassed catalyst samples under dynamic vacuum from 673 K to room temperature. This is the only step in the TPD experiment where readsorption of water could in principle occur. A possible explanation for the excess water occurring during the TPD experiment is the following: 673 K and high dynamic vacuum ($<1.33 \times 10^{-3}$ Pa) are not enough to desorb all chemisorbed water from the molecular sieves; some strongly chemisorbed water remains on the surface. When methanol adsorbs, a fast surface exchange reaction occurs between loosely bonded methanol and strongly bonded water (*19*):

$$H_2O\text{–}Z_1 + CH_3OH\text{–}Z_2 \rightleftarrows CH_3OH\text{–}Z_1 + H_2O\text{–}Z_2, \quad (2)$$

where Z_1 are strong adsorption sites and Z_2 weak adsorption sites.

During TPD the loosely bonded methanol and water desorb first and the strongly bonded methanol reacts to DME and hydrocarbons at higher temperatures. During these reactions the water formed desorbs in two steps: in the first step (dehydration of methanol to DME and water) we obtain 0.5

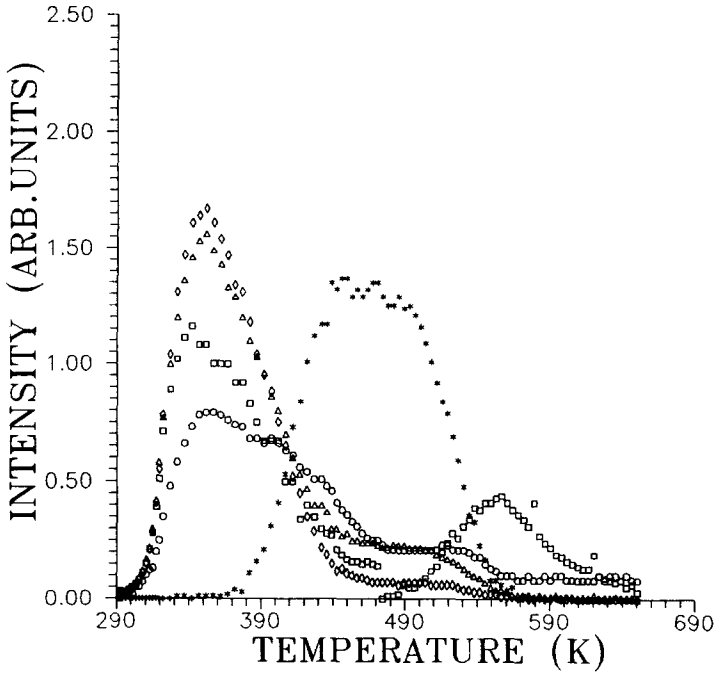

FIG. 3. TPD spectrum of methanol adsorbed on CoAPSO-34 molecular sieve, obtained by mass spectrometric analysis of evolved gases. For definitions of symbols, see Fig. 2 legend.

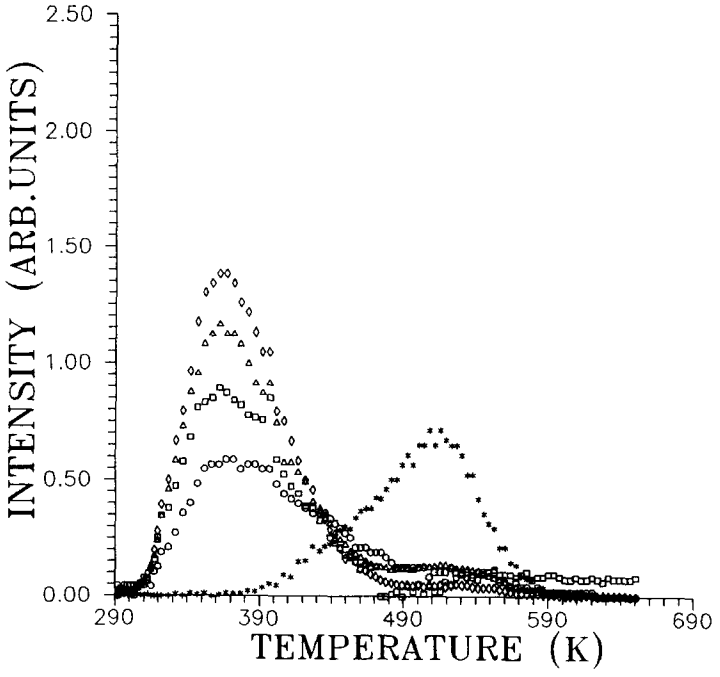

FIG. 4. TPD spectrum of methanol adsorbed on MnAPSO-34 molecular sieve, obtained by mass spectrometric analysis of evolved gases. For definitions of symbols, see Fig. 2 legend.

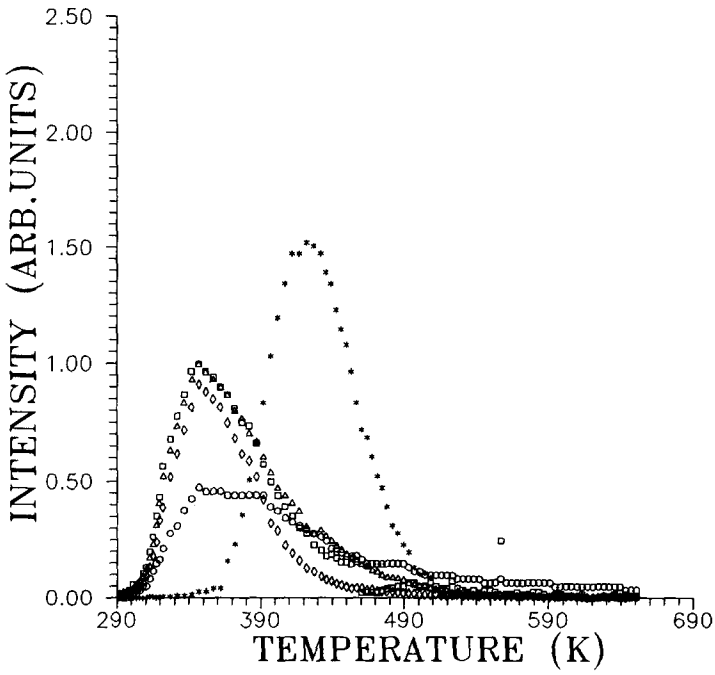

FIG. 5. TPD spectrum of methanol adsorbed on CrAPSO-34 molecular sieve, obtained by mass spectrometric analysis of evolved gases. For definitions of symbols, see Fig. 2 legend.

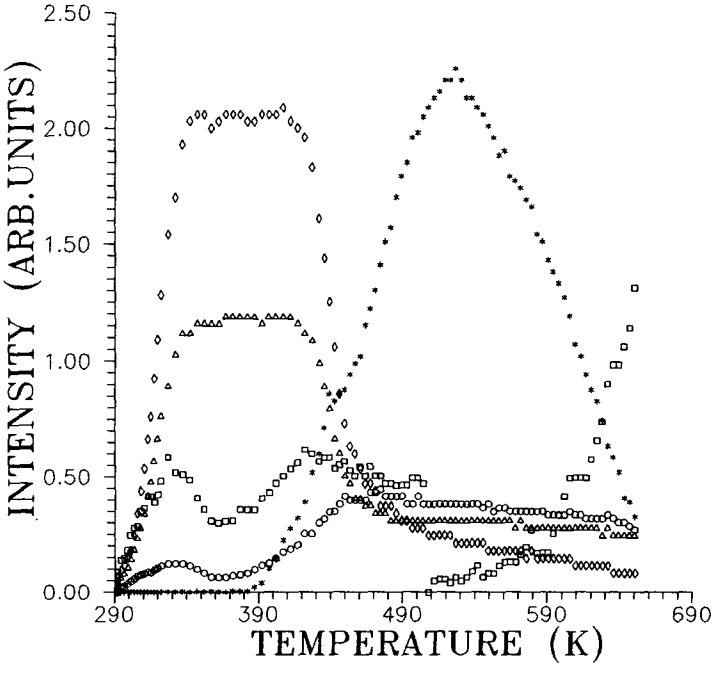

FIG. 6. TPD spectrum of methanol adsorbed on H-ZSM-5 molecular sieve, obtained by mass spectrometric analysis of evolved gases. Symbols the same as those in Fig. 2, except that $m/e = 45$ is enlarged 10 times.

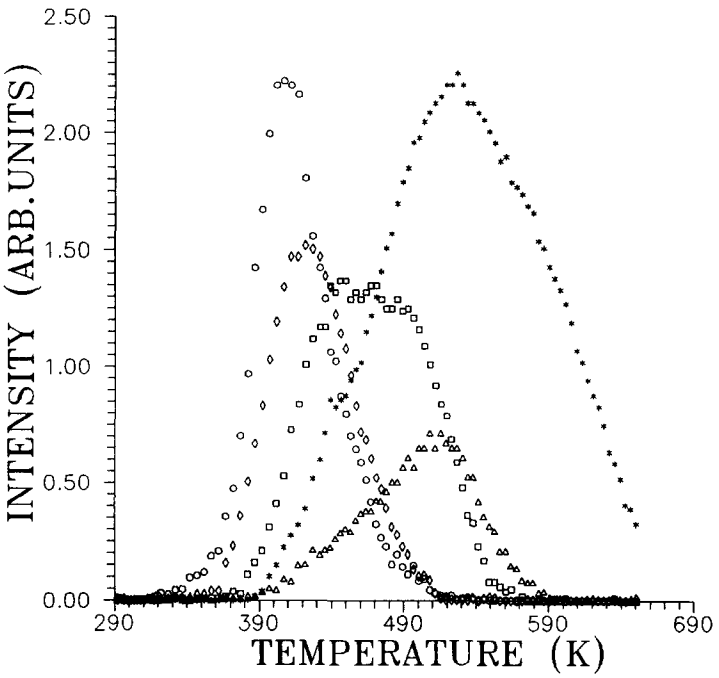

FIG. 7. Desorption curves of dimethyl ether (m/e = 45) obtained during TPD of methanol adsorbed on molecular sieves. (○) SAPO-34; (□) CoAPSO-34; (△) MnAPSO-34; (◇) CrAPSO-34; (∗) H-ZSM-5.

mol of water per mol of converted methanol, and in the second step (dehydration of DME to hydrocarbons and water) we obtain additionally 0.5 mol of water per mol of converted methanol. The mass balance equations for the whole process can be written as follows:

$$n\mathrm{CH_3OH} + d\mathrm{H_2O} \rightarrow (n - 2a)\mathrm{CH_3OH} + (a - b)(\mathrm{CH_3})_2\mathrm{O} + c\mathrm{C_2H_4} + (a + b + d)\mathrm{H_2O} + (b - c)\mathrm{C_2H_4}\ (\mathrm{coke}) \quad (3)$$

$$m = n + d + c \quad (4)$$

$$X_1 = (n - 2a)/m \quad (5)$$

$$X_2 = (a - b)/m \quad (6)$$

$$X_3 = c/m \quad (7)$$

$$X_4 = (a + b + d)/m \quad (8)$$

$$X_1 + X_2 + X_3 + X_4 = 1 \quad (9)$$

$$32 \cdot 2a = 18 \cdot (a + b) + 46 \cdot (a - b) + 28 \cdot b \quad (10)$$

$$32 \cdot m = 32 \cdot (n - 2a) + 46 \cdot (a - b) + 28 \cdot c + 18 \cdot (a + b + d). \quad (11)$$

The system of algebraic equations (4)–(11) is solved with n being the constant (gravimetrically determined quantity of adsorbed methanol in mol/g cat) and the X_1, X_2, X_3, X_4 being the initial values of molar fractions of evolved gases (determined by mass spectrometric analysis). The measured ion current of gas G evolved during TPD as a function of temperature is given by (*20*)

$$i_G^+(T) = \frac{i_{G(M)}^+(T)}{FF_{G(M)} \times XF_G}, \quad (12)$$

where $i_{G(M)}^+(T)$ is the ion current of the ion with $m/e = M$ of gas G, $FF_{G(M)}$ is the fragmentation factor for ion with $m/e = M$ of gas G, and XF_G is the relative probability of ionization of gas G at 70 eV electron energy. The molar fraction of gas G evolved during TPD is

$$X_G = \frac{\int_{T_1}^{T_2} i_G^+(T)\,dT}{\sum_{G=1}^{G=k} \int_{T_1}^{T_2} i_G^+(T)\,dT}. \quad (13)$$

The number of moles of evolved gas species calculated from the mass balance equations (4)–(11) is given by

$$m = \frac{\text{weight loss during TGA (g/g cat)}}{\sum_{G=1}^{G=k} M_G \times X_G^{\text{calc.}}} \text{ (mol/g cat)}, \quad (14)$$

where M_G is the molar mass of gas G and $X_G^{\text{calc.}}$ are the calculated molar fractions defined by Eqs. (5)–(8). The product composition is then given by

$$W_G = \frac{M_G \times X_G^{\text{calc.}} \times 100}{\sum_{G=1}^{G=k} M_G \times X_G^{\text{calc.}}} \text{ (wt\% of } CH_3OH \text{ adsorbed)}. \quad (15)$$

Thus the amounts of gaseous species evolved were obtained by integrating the TPD peaks in corresponding temperature intervals using the TGA to calibrate the peak areas. The results of these calculations are given in Table 3. Row 1 shows the quantity of adsorbed methanol (n), row 2 the calculated sum of moles of desorbed species (m), rows 3–7 the calculated composition of products, and rows 8 and 9 the calculated conversions of methanol and dimethyl ether (these are calculated as $\chi_{(CH_3OH)} = 2a/n$ and $\chi_{((CH_3)_2O)} = b/a$).

TABLE 2

Quantity of Methanol that Remains Adsorbed after Degassing of Samples at 293 K, Quantity (TG), and Composition (MS) of Desorbed Species during TPD between 293 and 673 K

Sample	Methanol ads. (g/g)	Species des. (g/g)	Composition of des. prod. (molar fractions)			
			CH_3OH	H_2O	C_2H_4	$(CH_3)_2O$
SAPO-34	0.034	0.036	0.44	0.53	0.024	0.009
CoAPSO-34	0.035	0.035	0.50	0.46	0.034	0.007
MnAPSO-34	0.014	0.017	0.58	0.40	0.015	0.004
CrAPSO-34	0.021	0.021	0.47	0.51	0.011	0.009
H-ZSM-5	0.026	0.024	0.65	0.24	0.031	0.083

Table 4 gives the concentration of isomorphously substituted elements (in moles per gram of catalyst) in SAPO-34 and MeAPSO-34 samples and the concentration of Al in the H-ZSM-5 sample as the elements building up the active centers of the type T_1-(OH)-T_2, where T_1 = Al, Co, Mn, Cr and T_2 = Si, P, respectively (*7*); the T–O bond distances of these elements (*7*); the experimentally determined temperatures of dimethyl ether desorption peaks; the molar ratios of desorbed dimethyl ether to desorbed methanol, calculated from the data given in Table 2; the reaction rates of methanol dehydration, calculated from the experimentally determined conversions of methanol in a gradientless reactor at the conditions described above (see Experimental section) (in moles of methanol per gram of catalyst per hour).

From the comparison of the quantities of adsorbed methanol (Table 3, row 1) and the quantities of elements incorporated in the framework of molecular sieves (Table 4, column 2) we can state that methanol forms 1 : 2 surface stoichiometric complexes on SAPO-34 and CrAPSO-34 (where Cr is not incorporated in the framework but blocks part of the active centers formed by incorporated Si (*13*)) with respect to the framework silicon. It forms a 1 : 1 stoichiometric surface complex in H-ZSM-5 with respect to the framework aluminum and the stoichiometry of the surface complexes formed in CoAPSO-34 and MnAPSO-34 remains ambiguous. It is probable, however, that on these two molecular sieves it also forms the 1 : 1 complexes with respect to the framework Co and Mn because of the need of Co and Mn, being tetrahedrally coordinated to framework oxygen ions, to complete their coordination sphere to the more stable octahedral one.

The stoichiometric surface complex of methanol and Brønsted acid sites in H-ZSM-5 has been well established by using the same adsorption–desorption technique as in the present paper (*15, 17*). It was also confirmed by IR spectroscopy that metha-

TABLE 3

Detailed Mass Balance of TPD Process and Conversions of Methanol and Dimethyl Ether

	SAPO-34	CoAPSO-34	MnAPSO-34	CrAPSO-34	H-ZSM-5
n [mol/g]	1.06×10^{-3}	1.09×10^{-3}	4.37×10^{-4}	6.56×10^{-4}	8.13×10^{-4}
m [mol/g]	1.38×10^{-3}	1.37×10^{-3}	5.30×10^{-4}	8.42×10^{-4}	8.77×10^{-4}
	Products composition (wt% of CH_3OH adsorbed)				
CH_3OH	57.0	62.5	70.3	60.3	70.3
H_2O	23.5	20.4	16.4	21.7	11.9
$(CH_3)_2O$	1.5	1.2	0.8	1.5	12.5
C_2H_4	2.6	3.7	1.6	1.2	2.7
Residuals[a]	15.2	11.9	10.9	15.2	2.7
X_{CH_3OH}	0.427	0.373	0.297	0.397	0.299
$X_{(CH_3)_2O}$	0.954	0.956	0.963	0.942	0.415

[a] Higher hydrocarbons and coke (calculated on the basis of C_2H_4).

nol in this surface complex is protonated (*15*). TPD studies of *n*-propylamine adsorbed on SAPO-5 (*21*) revealed that the measured acid site concentration reaches about 50% of the nominal number of isomorphously substituted Si atoms at the Si substitution level (Si/(Al + P + Si)) of about 0.08. This is in agreement with our findings that the concentration of adsorbed methanol per gram of SAPO-34 amounts to 50% of the nominal concentration of substituted Si per gram of SAPO-34 (see Tables 2 and 4). The chemical composition of SAPO-34 (Table 1) supports the prevailing presence of SM2 and little SM3 (Si + P > 0.5 and Al < 0.5) substitution mechanisms for Si incorporation (*7*). The potential number of Brønsted acid sites generated by Si isomorphous substitution is evidently reduced by the proportion of Si incorporated by SM3. However, even if only SM2 were present, there still exists the possibility that Si forms proton–donor centers of type I:

$$[(SiO)_{4-n}Si(OAl)_n]^{n-} \cdot nH^+ \quad \text{(I)}$$

with a different number of Al atoms (n) in the second coordination sphere of incorporated Si. It is well known from low-silica zeolite chemistry that centers with $n = 4$ and $n = 3$ have very low acid strengths and are incapable of protonating adsorbed bases (*22*). It seems that in the case of SAPO-34, where the SM2 mechanism of Si isomorphous substitution dominates, the number of proton–donor centers of type I with $n = 1$ and $n = 2$, capable of protonating methanol, is about half of all centers formed. The SAPO molecular sieves have therefore lower acid strengths than high-silica zeolites like H-ZSM-5 (*7*), where mainly proton–donor centers with $n = 1$ exist.

In the MeAPSO-34 systems one has a combination of Me–(OH)–P and Si–

TABLE 4

The Concentration of Active Centers in Catalysts, *T*–O Distances of Isomorphously Substituted Elements Forming the Active Centers, TPD Peak Temperatures for Dimethyl Ether Desorption, Molar Ratio of Desorbed Dimethyl Ether to Desorbed Methanol, and Reaction Rates for Methanol Dehydration at 623 K and 0.18 MPa

Sample	Conc. of elements (mol/g cat)	d_{T-O} (Å)	T_{des} (K)	DME/*M*	Reac. rate (mol/g h)
SAPO-34	2.14×10^{-3}(Si)	1.62(Si–O)	402	0.021	0.19
CoAPSO-34	1.26×10^{-3}(Co)	1.94(Co–O)	490	0.014	0.10
MnAPSO-34	0.65×10^{-3}(Mn)	2.02(Mn–O)	508	0.007	0.08
CrAPSO-34	1.31×10^{-3}(Si)[a]	1.84(Cr–O)	417	0.019	0.11
H-ZSM-5	0.83×10^{-3}(Al)	—	525	0.128	0.54

[a] Calculated under the assumption that Cr is not incorporated in the framework of molecular sieve but functions as the extraframework trivalent species that blocks the active centers, formed by Al–O–Si bonds.

(OH)–Al Brønsted acid sites. The MO calculations of acidity of SAPO and MeAPO molecular sieves (*23*) reveal that Me–(OH)–P groups are more acidic than Si–(OH)–Al groups. The frequency of the hydroxyl stretching vibration band of the Mg–(OH)–P group in MgAPSO is 26 cm^{-1} lower than the frequency for the Si–(OH)–Al group (*7*). TPD studies of adsorbed ammonia and *n*-propylamine on SAPO, MeAPO, MeAPSO, and H-ZSM-5 have shown that the substituted aluminophosphate molecular sieves have lower acid strengths than H-ZSM-5 (*21*). The DME desorption peaks on our TPD spectra (Fig. 7) show, indeed, that the Me–(OH)–P groups in MeAPSO-34 samples are more acidic than the Si–(OH)–Al groups in SAPO-34 and MeAPSO-34, but less than the Si–(OH)–Al groups in H-ZSM-5. Comparing the quantities of adsorbed methanol (Table 2) and the concentrations of transition elements in MeAPSO-34 molecular sieves (Table 4), one can conclude that methanol is adsorbed on more acidic Me–(OH)–P sites preferentially.

The fine structure of the water desorption profile during TPD of methanol contains important information by which we can follow the energetic heterogeneity of adsorption sites and the reaction sequence quantitatively. This is clearly visible by closer inspection of the water desorption spectra from CoAPSO-34 and H-ZSM-5 samples. The desorption spectrum of water from the CoAPSO-34 sample has four overlapped peaks (see Fig. 3). The low-temperature peak is assignable to desorption of water due to a surface exchange reaction with adsorbed methanol, as explained above. Then follow two consecutive desorption peaks that belong to desorption of water produced during the methanol dehydration to DME on two energetically nonequivalent active sites (*24*). The high-temperature desorption peak belongs to the water produced during the DME dehydration to ethene.

The desorption spectrum of water during TPD of methanol on the H-ZSM-5 sample has two distinct low-temperature peaks that appear simultaneously as the two low-temperature peaks in the desorption spectrum of unconverted methanol (see Fig. 6). These two peaks belong to energetically nonequivalent adsorption sites (low Si/Al ratio $\cong$ 19 gives the possibility that there are two types of adsorption sites connected with Si(0Al) and Si(1Al) or that during calcination some extraframework Al formed). The next two peaks, due to both reaction sequences of methanol dehydration in which water is produced, are overlapped and cannot be distinguished.

The peaks are present also in the water desorption spectra of other samples, but they are less pronounced.

The next very clearly visible feature on the TPD spectra is the temperature shifts of the DME desorption spectra for different samples (see Fig. 7). Although the SAPO-34 and MeAPSO-34 samples are isostructural, the isomorphous substitution of framework elements caused slight changes in the geometry of channel apertures as well as changes in the distribution of concentration and strength of adsorption sites in the framework. All these changes should in principle have an influence on the diffusivity of the adsorbate (DME in this case) in the crystals of molecular sieves. The changes in the geometry of channel apertures between the SAPO-34 and MeAPSO-34 samples are however negligible. As an example, the mean of the squares of 8-membered ring diameters (i.e., the distances between the centers of oxygen atoms in the nearly circular eight-membered rings less the doubled radius of the oxygen ion (0.244 nm) (*7*)) of SAPO-34 and CoAPSO-34, determined from the single-crystal X-ray diffraction data on SAPO-34 (*25*) and CoAPSO-34 (*24*), are 0.4300 nm and 0.4304 nm, respectively. Within the homologous series of SAPO-34 and MeAPSO-34 samples, therefore, we cannot speak about the diffusional limitations as a reason for differences in DME desorption peak temperatures. There is another strong experimental evidence in sup-

port of this. Namely, if the sequence of DME desorption peak temperatures were a consequence of diffusional limitations, then DME would desorb from H-ZSM-5 at a lower temperature than it would desorb from the chabazite-like SAPO-34 and MeAPSO-34 structures, since the 10-membered ring channel apertures in the MFI structure are wider than the 8-membered ring apertures in the CHA-like structures. The experimental facts show a quite opposite picture (see Fig. 7).

The influence of the isomorphously substituted elements on the strength of DME-adsorbent interaction is however clearly evident from the TPD spectra. The stronger this interaction, the higher the DME desorption peak temperature. The onset and peak temperatures on the DME desorption kinetic curves follow the same sequence of samples: H-ZSM-5 > MnAPSO-34 > CoAPSO-34 > CrAPSO-34 > SAPO-34. This sequence can be regarded as a sequence of acid strength. It clearly demonstrates that the second reaction step (dehydration of DME to hydrocarbons) involves as catalytically active centers those formed by isomorphously substituted elements in the framework of molecular sieves.

If there are several types of energetically different adsorption sites, the desorption kinetic curve will be in principle composed of several more or less overlapping peaks. This is illustrated by the DME desorption kinetic curve for the CoAPSO-34 sample, where there are two overlapping peaks consistent with the above discussion of water desorption kinetic curves. On the same basis we can say that the DME desorption kinetic curve for H-ZSM-5 consists of two overlapping peaks that are, however, less resolved than in the case of the CoAPSO-34 sample.

The desorption spectra of species having $m/e = 28$ that were ascribed to the ethene parent ion (see the Experimental section) deserve special attention. These species begin to desorb at temperatures higher than the DME desorption peak temperatures. The sequence of desorption peak temperatures during TPD of methanol is thus $T_{H_2O} \approx T_{CH_3OH} < T_{(CH_3)_2O} < T_{C_2H_4}$. This sequence follows from the well-known fact that in catalytic methanol dehydration at low temperatures the reaction proceeds so as to produce only DME and water. At higher temperatures, provided the catalysts have strong enough Brønsted acid sites, the reaction proceeds further to form hydrocarbons and water by dehydration of DME (*2*). The only difference in the sequence of product appearance as a function of reaction temperature between the usual measurements in a catalytic reactor (*26*) and our TPD experiments is in the appearance of a low-temperature water desorption peak, and the plausible explanation for this was given above. It is interesting to note that the onset temperatures of ethene desorption peaks, about 460 K (see Figs. 2–6), are in very good agreement with the temperature of ethene appearance among the products of DME dehydration in a catalytic reactor loaded with H-ZSM-5 catalyst (product distribution versus reaction temperature) (*26*). This means that in TPD experiments carried out with a heating rate of 10 K/min the attainment of stationary states is fast.

In the chabazite-like structures the narrow windows of the cages prevent the diffusion of longer normal and isoalkanes and alkenes or aromatics, which form in the cavities, to the surface of the crystals, thus giving rise to the conditions for molecular shape selectivity to products. The species that can diffuse through these windows must have kinetic diameters less than approximately 0.43 nm (*14, 27*). The kinetic diameters of species found in the gaseous phase in our reaction system are: methanol (0.363 nm), dimethyl ether (0.431 nm), water (0.264 nm), ethene (0.416 nm), are ethane (0.444 nm) (*28*). The species with longer chains have larger kinetic diameters (e.g., propene has 0.468 nm) and would hardly diffuse out from the chabazite cages. If the acid strength of the catalytically active centers can be matched appropriately, so that the second reaction step of methanol dehydra-

TABLE 5

Ethene Selectivities Obtained from TPD and Catalytic Measurements

Sample	Selectivity toward C_2H_4 (C-wt%)	
	TPD	CST reactor
SAPO-34	10.6	6.1
CoAPSO-34	17.3	12.0
MnAPSO-34	24.1	18.6
CrAPSO-34	8.7	9.9
H-ZSM-5	56.8	40.8

tion can start, such a catalytic system would produce ethene selectively. It seems that this is the case with MnAPSO-34, which gives the highest selectivity for ethene (see Table 5).

The catalytic activity sequence as determined with a gradientless reactor at 623 K and 1.8 bar is the following: H-ZSM-5 > SAPO-34 > CrAPSO-34 > CoAPSO-34 > MnAPSO-34. The main products in the catalytic systems with SAPO-34 and MeAPSO-34 were DME and water with a small (less than 1 mol%) amount of short chain hydrocarbons, mainly ethene. The observed catalytic activity sequence is consistent with the hypothesis (*29*) that the first reaction step in methanol dehydration depends on cumulative Brønsted acidity so that it is proportional to the concentration of acid centers irrespective of their acid strength (see Table 4). The catalytic activity in the second reaction step, however, depends on the acid strength. It should be pointed out that the reaction rates were determined at high WHSV values (26.6 h^{-1}), where the conversion of methanol was relatively low (around 10%). The selectivities for the formation of low olefins decrease rapidly with time on stream for all catalysts in the SAPO-34 and MeAPSO-34 series as a consequence of coking. In fact, the used samples of catalysts were black with coke after exposure to methanol for about 6 h.

Table 3 gives valuable information about the composition of products in TPD. The most striking difference between H-ZSM-5 on one hand and SAPO-34 and MeAPSO-34 on the other is that the latter undergo severe coking during TPD. However, from TPD studies (Table 3) one obtains higher conversions of methanol and twice as high conversions of DME to hydrocarbons on SAPO-34 and MeAPSO-34 samples in comparison with H-ZSM-5. These differences are certainly not a consequence of the differences in the number of active sites per gram of catalyst or the differences in their acid strength; they are a consequence of the different structures of the molecular sieves. The channel structures, like that of ZSM-5, seem to be less exposed to coking, while in the cage structures, like those of SAPO-34 and MeAPSO-34, the coking is severe and makes these structures less suitable for dehydration catalysts.

The data in Table 4 enable comparison of chemical analysis results (concentration of isomorphously substituted elements), TPD (DME desorption peak temperatures and molar ratios of desorbed DME to desorbed methanol), and reaction rate measurements. It is very interesting to note that the temperatures of DME desorption peaks in the series of isostructural samples (SAPO-34 and MeAPSO-34) correlate with the *T*–O distances of the isomorphously substituted elements, except for CrAPSO-34, where Cr obviously is not incorporated into the framework (*13*) (see Fig. 8). More than that, the molar ratios of desorbed DME to desorbed methanol calculated from TPD spectra correlate satisfactorily with reaction rates measured with the gradientless reactor. From the product composition given in Table 3 one can calculate the weight percent of ethene in hydrocarbon products (coke included) and normalize this with respect to the concentration of desorbed species per gram of catalyst. Values recalculated in this manner represent the selectivities for ethene as obtained from TPD measurements and can be compared with the values of weight percent of ethene in hydrocarbon products

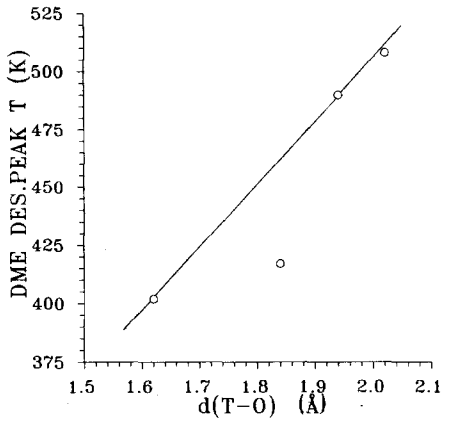

FIG. 8. Correlation of DME desorption peak temperatures and interatomic T–O distances for SAPO-34 and MeAPSO-34 (Me = Cr, Mn, Co).

(coke excluded) calculated from the product distribution obtained with a gradientless catalytic reactor. These selectivities are presented in Table 5. The highest selectivity determined by both methods is that of H-ZSM-5. Among the aluminophosphate catalysts the highest selectivity is obtained for the MnAPSO-34 sample.

Comparing our results on SAPO-34 with those published in the literature (*8*, *9*) we need to state that the feed composition, reaction conditions (reaction temperature, pressure, space velocity), and the type of reactor used in our study are entirely different from those used by Liang *et al.* (*9*) and by Inui *et al.* (*8*). At 8000 h^{-1} (GHSV), reaction temperature 295°C, total pressure of 1 bar, methanol partial pressure of 0.20 atm (balance gas N_2), methanol conversion 60.5%, Inui *et al.* (*8*) obtained a selectivity of about 24 C-wt% of ethene in hydrocarbons in a continuous-flow tubular reactor. Liang *et al.* (*9*) also used a continuous-flow tubular reactor with feed composition 30 CH_3OH : 70 H_2O, at WHSV = 3.6 h^{-1}, reaction temperature 406°C, total pressure 1 bar, methanol conversion 100% and obtained a selectivity of 30.8 C-wt% of ethene in hydrocarbons. In our CST reactor at the feed composition 80 CH_3OH : 20 N_2, total pressure 1.8 bar, reaction temperature 350°C, WHSV = 26.6 h^{-1}, methanol conversion 20.6%, we obtained a selectivity of 6.1 C-wt% of ethene in hydrocarbons. The relatively low ethene selectivity that we obtained in the CST reactor was confirmed also by the TPD of methanol (see Table 5).

CONCLUSIONS

The information obtained from temperature-programmed desorption spectra of methanol on molecular sieves SAPO-34, MeAPSO-34 (Me = Co, Mn, Cr), and H-ZSM-5 gives the following details of the catalytic behavior of these materials:

—the strength of acid sites;
—the concentrations of acid sites of different strength;
—the relative catalytic activity of samples within a series of homologues;
—the selectivity toward different products;
—information about successful or unsuccessful incorporation of the active centers forming elements in the framework.

This is shown to be in accordance with the catalytic activity and selectivity data obtained from measurements of methanol dehydration reaction rates in a gradientless catalytic reactor.

The measured acid strength of the catalysts follows the sequence: H-ZSM-5 > MnAPSO-34 > CoAPSO-34 > CrAPSO-34 > SAPO-34. The measured catalytic activity follows the sequence: H-ZSM-5 ≫ SAPO-34 > CrAPSO-34 > CoAPSO-34 > MnAPSO-34. The isomorphously substituted aluminophosphate molecular sieves deactivate rapidly with time on stream as a consequence of coking. The highest selectivity to ethene production among these samples was found for MnAPSO-34.

ACKNOWLEDGMENTS

The authors are grateful to Mr. Edvard Židan for the reaction rate measurements with the gradientless catalytic reactor. Financial support of the National Slovene Board for Science and Technology (RSRDT), Grant No. C2-0538-104, is gratefully acknowledged.

REFERENCES

1. Meisel, S. L., McCullough, J. P., Lechthaler, C. H., and Weisz, P. B., *Chemtech* **6,** 86 (1976).
2. Chang, C. D., Hydrocarbons from Methanol, Chemical Industries Vol. 10, Marcel Dekker, Inc., New York, 1983.
3. Kaeding, W. W., and Butter, S. A., *J. Catal.* **61,** 155 (1980).
4. McIntosh, R. J., and Seddon, D., *Appl. Catal.* **6,** 307 (1983).
5. Chang, C. D., Lang, W. H., and Silvestri, A. J., US Patent 4,062,905 (1977).
6. Wilson, S. T., Lok, B. M. T., and Flanigen, E. M., EP 0 043 562 (1982).
7. Flanigen, E. M., Patton, R. L., and Wilson, S. T., *Stud. Surf. Sci. Catal.* **37,** 13 (1988).
8. Inui, T., Matsuda, H., Okaniwa, H., and Miyamoto, A., *Appl. Catal.* **58,** 155 (1990).
9. Liang, J., Li, H., Zhao, S., Guo, W., Wang, R., and Ying, M., *Appl. Catal.* **64,** 31 (1990).
10. Inui, T., Phatanasri, S., and Matsuda, H., *J. Chem. Soc. Chem. Commun.,* 205 (1990).
11. Romannikov, V. N., Mastikhin, V. M., Hočevar, S., and Držaj, B., *Zeolites* **3,** 311 (1983).
12. Rajić, N., Kaučič, V., and Stojaković, D., *Zeolites* **10,** 169 (1990).
13. Rajić, N., Žagar, T., and Kaučič, V., "Studies of MeAPSO molecular sieves (Me = Co^{2+}, Mn^{2+}, Cr^{3+}) with chabazite structure," presented at 13th Annual Meeting, British Zeolite Association, Chislehurst, 1990.
14. Lok, B. M., Messina, C. A., Patton, R. L., Gajek, R. T., Cannan, T. R., and Flanigen, E. M., US Patent 4,440,871 (1984).
15. Aronson, M. T., Gorte, R. J., and Farneth, W. E., *J. Catal.* **98,** 434 (1986).
16. Cornu, A., and Massot, R., "Compilation of Mass Spectral Data," Heyden, London, 1966.
17. Biaglow, A. I., Gittleman, C., Gorte, R. J., and Madon, R. J., *J. Catal.* **129,** 88 (1991).
18. Kollen, W., and Vasofsky, R., *in* "Microweighing in Vacuum and Controlled Environments" (A. W. Czanderna and S. P. Wolsky, Eds.), pp. 233–260. Elsevier, Amsterdam, 1980.
19. Rozovskii, A. Ya., *Kinet. Katal.* **30**(3), 533 (1989).
20. Doebler, U., "Quantitative Mass Spectrometry," Seminar Handbook of Leybold AG, Köln, 1990.
21. Tapp, N. J., Milestone, N. B., and Bibby, D. M., *Stud. Surf. Sci. Catal.* **37,** 393 (1988).
22. Ione, K. G., and Vostrikova, L. A., *Usp. Khim.* **16,** 393 (1987).
23. Carson, R., Cooke, E. M., Dwyer, J., Hinchliffe, A., and O'Malley, P. J., *Stud. Surf. Sci. Catal.* **46,** 39 (1989).
24. Nardin, G., Randaccio, L., Kaučič, V., and Rajić, N., *Zeolites* **11,** 192 (1991).
25. Ito, M., Shimoyama, Y., Saito, Y., Tsurita, Y., and Otake, M., *Acta Crystallogr. C* **41,** 1698 (1985).
26. van Hooff, J. H. C., van den Berg, J. P., Wolthuizen, J. P., and Volmer, A., *in* "Proceedings, 6th International Zeolite Conference" (D. Olson and A. Bisio, Eds.), pp. 489–496. Butterworths, Guildford, UK, 1984.
27. Lok, B. M., Messina, C. A., Patton, R. L., Gajek, R. T., Cannan, T. R., and Flanigen, E. M., *J. Am. Chem. Soc.* **106,** 6092 (1984).
28. Reid, R. C., Prausnitz, J. M., and Poling, B. E., "The Properties of Gases and Liquids," 4th ed. pp. 733–734. McGraw–Hill, New York, 1987.
29. Hočevar, S., and Držaj, B., *J. Catal.* **73,** 205 (1982).